Ion access pathway to the transmembrane pore in P2X receptor channels

Toshimitsu Kawate,[1] Janice L. Robertson,[2] Mufeng Li,[1] Shai D. Silberberg,[1] and Kenton J. Swartz[1]

[1]Porter Neuroscience Research Center, Molecular Physiology and Biophysics Section, National Institute of Neurological Disorders and Stroke, National Institutes of Health, Bethesda, MD 20892
[2]Department of Biochemistry, Howard Hughes Medical Institute, Brandeis University, Waltham, MA 02454

P2X receptors are trimeric cation channels that open in response to the binding of adenosine triphosphate (ATP) to a large extracellular domain. The x-ray structure of the P2X4 receptor from zebrafish (zfP2X4) receptor reveals that the extracellular vestibule above the gate opens to the outside through lateral fenestrations, providing a potential pathway for ions to enter and exit the pore. The extracellular region also contains a void at the central axis, providing a second potential pathway. To investigate the energetics of each potential ion permeation pathway, we calculated the electrostatic free energy by solving the Poisson-Boltzmann equation along each of these pathways in the zfP2X4 crystal structure and a homology model of rat P2X2 (rP2X2). We found that the lateral fenestrations are energetically favorable for monovalent cations even in the closed-state structure, whereas the central pathway presents strong electrostatic barriers that would require structural rearrangements to allow for ion accessibility. To probe ion accessibility along these pathways in the rP2X2 receptor, we investigated the modification of introduced Cys residues by methanethiosulfonate (MTS) reagents and constrained structural changes by introducing disulfide bridges. Our results show that MTS reagents can permeate the lateral fenestrations, and that these become larger after ATP binding. Although relatively small MTS reagents can access residues in one of the vestibules within the central pathway, no reactive positions were identified in the upper region of this pathway, and disulfide bridges that constrain movements in that region do not prevent ion conduction. Collectively, these results suggest that ions access the pore using the lateral fenestrations, and that these breathe as the channel opens. The accessibility of ions to one of the chambers in the central pathway likely serves a regulatory function.

The Journal of General Physiology

Downloaded from http://rupress.org/jgp/article-pdf/137/6/579/1914952/jgp_201010593.pdf by guest on 10 February 2026

INTRODUCTION

P2X receptors are cation-permeable channels that play crucial roles in extracellular ATP-mediated signaling (North, 2002; Burnstock, 2006). These receptors are widely expressed throughout the human body and play important roles in cell–cell communication, ranging from sensory signal transduction (Cook et al., 1997; Finger et al., 2005) to immune responses (Solle et al., 2001; Chessell et al., 2005). Malfunction of P2X receptor–mediated ATP signaling is implicated in various pathological conditions, including neuropathic pain (Souslova et al., 2000; Dell'Antonio et al., 2002; Tsuda et al., 2003) and inflammatory diseases such as asthma and arthritis (Dowd et al., 1998; Idzko et al., 2007). Therefore, P2X receptor channels are promising targets for the development of new therapeutic agents.

P2X receptor channels are composed of three subunits that assemble as either homomeric or heteromeric complexes of seven different subunits (P2X1–7) (Nicke et al., 1998; Vial et al., 2004). Each of the three subunits of P2X receptors has two transmembrane helices, which link the intracellular amino and carboxyl termini to the large extracellular region (~280 amino acids). These architectural features distinguish P2X receptors from the other ligand-gated cation channels, which include tetrameric glutamate receptors (Rosenmund et al., 1998; Sobolevsky et al., 2009) and pentameric acetylcholine receptors (Reynolds and Karlin, 1978; Unwin, 2005). The recent crystal structure of a closed P2X4 receptor from zebrafish (zfP2X4) revealed that this large extracellular region has a novel architecture among the available ion channel structures, harboring three potential ATP-binding pockets, disulfide-rich motifs, and conspicuous vestibules that form a void in the middle of three subunits (Kawate et al., 2009). Although accessibility and metal bridging experiments in rat P2X2 (rP2X2) support a TM2 helix-straightening model for opening of the pore (Kracun et al., 2010; Li et al., 2010), the accompanying structural

Correspondence to Toshimitsu Kawate: kawatet@ninds.nih.gov; or Kenton J. Swartz: swartzk@ninds.nih.gov

Abbreviations used in this paper: BK, large-conductance Ca^{2+}-activated K^+; hP2X5, human P2X5; MTS, methanethiosulfonate; MTSET, 2-(trimethylammonium)ethyl MTS; MTS-TPAE, 2-(tripentylammonium)ethyl MTS; rP2X2, rat P2X2; TR-MTSEA, Texas red-2-sulfonamidoethyl MTS; zfP2X4, P2X4 receptor from zebrafish.

This article is distributed under the terms of an Attribution–Noncommercial–Share Alike–No Mirror Sites license for the first six months after the publication date (see http://www.rupress.org/terms). After six months it is available under a Creative Commons License (Attribution–Noncommercial–Share Alike 3.0 Unported license, as described at http://creativecommons.org/licenses/by-nc-sa/3.0/).

The Rockefeller University Press $30.00
J. Gen. Physiol. Vol. 137 No. 6 579–590
www.jgp.org/cgi/doi/10.1085/jgp.201010593

rearrangements in the extracellular region remain relatively unexplored.

In this study, we investigated the pathway through which ions traverse the extracellular domain of P2X receptors to enter or exit the transmembrane pore. The x-ray structure of zfP2X4 reveals that two potential pathways exist. The first pathway is through three lateral fenestrations that connect the extracellular solution to an extracellular vestibule just above the occluded gate region of the pore (Fig. 1, A and B). Although these lateral fenestrations have dimensions of ~8 × 10 Å in the zfP2X4 receptor structure, several important side chains were not modeled because of the poor quality of electron density maps in this region (N54, D59, T60, Q329, I335, and I336 in zfP2X4). The inclusion of all side chains in the zfP2X4 structure suggests that these fenestrations may be somewhat narrower. The second possible pathway for ions to access the pore is along the central threefold axis of the zfP2X4 structure (Fig. 1, A and B). Two conspicuous electronegative cavities are present between the outermost end of the extracellular region and the extracellular vestibule in zfP2X4, which are predicted to form favorable sites for cation binding. Although the diameter of the pathways connecting these chambers with each other and the extracellular solution at the top of the receptor would not support rapid ion throughput, they might expand after the binding of ATP. There is precedence in other ion channels for both types of potential permeation pathways. Ions must traverse an extended (~85 Å) pore that projects into the cytoplasm in inward-rectifier potassium (Kir) channels (Nishida and MacKinnon, 2002; Nishida et al., 2007; Tao et al., 2009), and ions are thought to use four lateral fenestrations between the transmembrane pore and the cytoplasmic "hanging gondola" in voltage-activated potassium (Kv) channels (Kobertz and Miller, 1999; Long et al., 2007), and in corresponding regions in CNG channels (Johnson and Zagotta, 2005). To probe the ion access pathway in the extracellular region of a P2X receptor, we performed Cys-scanning mutagenesis and accessibility studies using methanethiosulfonate (MTS) reagents. In combination with disulfide cross-linking experiments and electrostatic energy calculations, our data suggest that ions do not use the central pathway, but likely permeate through the three lateral fenestrations located between the extracellular region and the transmembrane pore.

MATERIALS AND METHODS

Poisson-Boltzmann calculations

The zfP2X4 crystal structure (Protein Data Bank accession no. 3H9V) was modeled from residue 32 to 361, with missing side chains built using CHARMM. The rP2X2 receptor and the human P2X5 (hP2X5) receptor homology models were created based on the zfP2X4 receptor crystal structure using MODELLER software (Eswar et al., 2006). The electrostatic free energy of ion interaction along the two pathways was determined by calculating $\Delta\Delta G_{int} = \Delta G_{ion+channel} - \Delta G_{channel} - \Delta G_{ion}$, with each component obtained from a distinct numerical solution of the finite-difference Poisson-Boltzmann equation for the given system. This procedure ensures that the contribution from the static field (arising from the protein charges) and the reaction field (arising from the spatial variations in the dielectric constant) are both incorporated into the calculated free energy. The calculations were performed following the methods described in Robertson et al. (2008), using the PBEQ module in CHARMM (version 35a1) and the set of optimized atomic Born radii for amino acids (Nina et al., 1997; Im et al., 1998; Brooks et al., 2009). The zfP2X4, rP2X2, and hP2X5 systems were aligned with the central pore along the z axis. For the finite-difference Poisson-Boltzmann calculations, each system contained ~160 × 160 × 290 grid points with cell size of 1.0 Å focused to 0.5 Å. The membrane was defined as a 25-Å-thick slab centered at Z = 0 Å with dielectric constant $\varepsilon_M = 2$, whereas protein and solvent dielectric constants were set to $\varepsilon_P = 2$ and $\varepsilon_S = 80$, respectively. Ions were treated explicitly inside a box defined from −15 Å < X < 15 Å, −15 Å < Y < 15 Å, and −20 Å < Z < 90 Å, and Debye-Hückel ionic screening corresponding to 150 mM of salt was considered outside this region. All residues were set to their native protonation states, with histidines neutral. For the lateral fenestrations, $\Delta\Delta G_{int}$ was calculated for accessible points, those positions >2 Å from a protein atom, within a 20-Å radius of Z = 25 Å. The artificial opening of the central pore was constructed by carrying out an adopted basis Newton-Raphson minimization with a cylindrical potential resistant along the central axis of the protein, successively increasing the radius by 0.1 Å to a final radius of 5 Å.

Expression constructs and transfection

To avoid unwanted modification at native Cys, all mutants were introduced into the rP2X2-3T, where all three nondisulfide bridge–forming Cys (C9, C348, and C430) are mutated to threonine

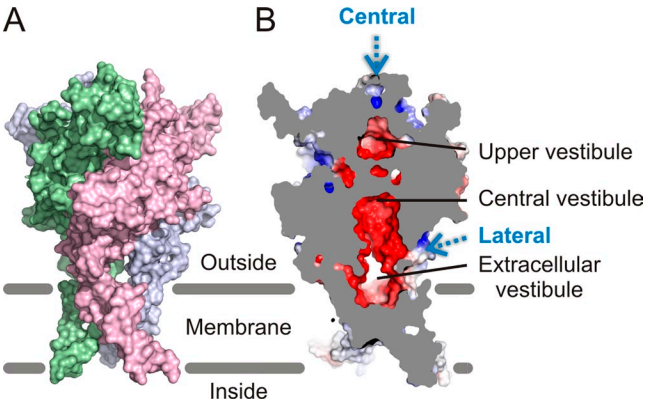

Figure 1. Two potential pathways for extracellular ions to access the transmembrane pore in P2X receptors. (A) Surface representation of the zfP2X4 receptor model in the closed state. Each color represents one of the three subunits. (B) A sagittal section of the closed-state model reveals two potential ion access pathways (central and lateral pathways; blue dashed arrows). Electrostatic potential surface calculated using the APBS tools (Baker et al., 2001) shows two acidic vestibules along these potential ion access pathways (upper and central vestibules). The surface is colored based on the potential, contoured from −6 kcal mol^{-1} (red) to +6 kcal mol^{-1} (blue). White denotes 0 kcal mol^{-1}. To complement the electrostatic contributions of the missing side chains in the crystal structure because of weak electron density, the side chains were added back to the model, and their geometry was optimized using the MODELLER software (Eswar et al., 2006). Structural representations in all figures were generated using PyMOL (Schrödinger, LLC).

Downloaded from http://rupress.org/jgp/article-pdf/137/6/579/1914952/jgp_201010593.pdf by guest on 10 February 2026

(Li et al., 2008). The parent rP2X2-3T was subcloned into the pIRES-EGFP RK6 vector (provided by M. Mayer, National Institutes of Health, Bethesda, MD) using BamHI and HindIII sites, modified to either single or double Cys mutants using the QuickChange technique (Agilent Technologies), and confirmed by DNA sequencing. For whole cell patch clamp recordings, HEK293 cells were split on glass coverslips in a six-well plate (Corning) at 5–10 × 10^4 cells/well, cultured in DMEM (Invitrogen) for 10–15 h at 37°C, transfected with 300–800 ng DNA per well using Fugene 6 reagent (Roche), and used 16–32 h after transfection. For Western blotting, ∼90% confluent HEK293 cells in six-well pates were transfected with 4 µg of DNA constructs/well using Lipofectamine 2000 reagent (Invitrogen) and used 48 h after transfection.

Whole cell patch clamp recording

Membrane currents were recorded from HEK293 cells using the whole cell patch clamp configuration. Membrane voltage was clamped at −60 mV with an Axopatch 200B patch clamp amplifier (Axon Instruments), currents were filtered at 2 kHz (eight-pole Bessel; model 900BT; Frequency Devices) and digitized online using a Digidata 1321A interface board and pCLAMP 10 software (Axon Instruments). The standard extracellular solution contained: 140 mM NaCl, 5.4 mM KCl, 2 mM $CaCl_2$, 0.5 mM $MgCl_2$, 10 mM HEPES, and 10 mM D-glucose, adjusted to pH 7.3 with NaOH. The pipette solution contained: 140 mM NaCl, 10 mM EGTA, and 10 mM HEPES, adjusted to pH 7.0 with NaOH. Bath and ground chambers were connected by an agar bridge containing 2 M KCl. Extracellular solutions were rapidly exchanged (∼50 ms) to ATP-containing solutions with and without MTS reagents using a computer-controlled perfusion system (RSC-200; Bio-Logic). Stock MTS reagents (bromide salt; Toronto Research Chemicals) were freshly made in H_2O at 100 mM (prepared every 4 h), stored on ice, and diluted to the desired concentrations within 2 min of their use in experiments. To expedite the screening process, we determined the titratable range of the concentration–response relation for ATP for each single and double Cys mutant by applying three different concentrations of ATP (e.g., 1, 10, and 100 µM). For each mutant, MTS accessibility was assessed using an ATP concentration near the EC_{50}, and all the recordings were performed for three or more cells.

Detection of intersubunit disulfide bridge formation

To obtain a high signal to noise ratio in Western blots, an octa-histidine tag (His_8) was attached to each of the double Cys mutants using PCR and standard molecular biology techniques. All such constructs behaved similarly to the ones without His_8 in whole cell patch clamp

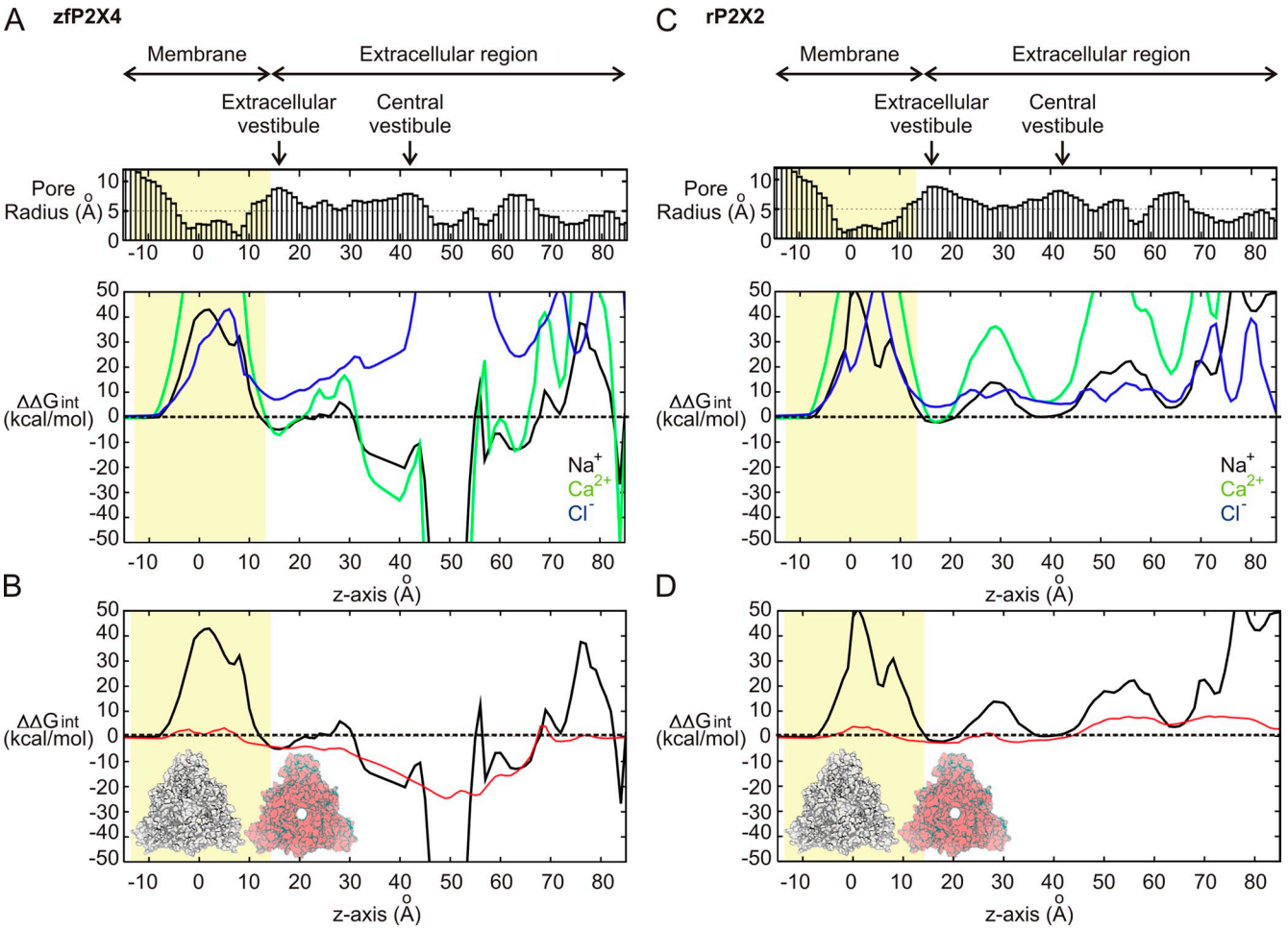

Figure 2. Electrostatic interaction free energy of ions along the central pathways in zfP2X4 and rP2X2. Results for zfP2X4 are shown in A and B, whereas those for rP2X2 are shown in C and D. (A and C) $\Delta\Delta G_{int}$ of Na^+ (black), Ca^{2+} (green), and Cl^- (blue), calculated along the central pathway, with the transmembrane region depicted with the yellow slab and the center of the membrane at Z = 0 Å. The pore radius profile is shown in the bar graph on top. (B and D) $\Delta\Delta G_{int}$ of Na^+ along the central pathway of the original closed model (black), and an artificially opened pore widened to 5-Å radius from the molecular threefold symmetry axis (red). The surface representations of the original closed (white) and the forced open (red) conformations are shown.

Downloaded from http://rupress.org/jgp/article-pdf/137/6/579/1914952/jgp_201010593.pdf by guest on 10 February 2026

recordings (not depicted). HEK293 cells expressing these double Cys mutants were washed with PBS, resuspended in 100 µl/well of S buffer (25 mM Tris, pH 7.4, 137 mM NaCl, 3 mM KCl, 20 mM *n*-dodecyl-β-maltoside, Complete Protease Inhibitor Cocktail [Roche], and 1 mM PMSF), rotated for 30 min at 4°C, and spun at 40,000 rpm in a TLA 100.3 rotor (Beckman Coulter) for 30 min. The soluble fraction (10 µl) was incubated with nonreducing SDS-PAGE sample buffer and resolved on a 4–12% Bis-Tris SDS-PAGE gel (Invitrogen). The double Cys mutants were detected by Western blotting using 1/500 dilution of anti-His monoclonal antibody (Thermo Fisher Scientific), 1/1,000 dilution of anti–mouse secondary antibody conjugated with alkaline phosphatase (Bio-Rad Laboratories), and Colorimetric AP substrate (Bio-Rad Laboratories).

RESULTS

The objective of this study was to identify the permeation pathway for ions through the extracellular region of P2X receptor channels. We chose to use the rP2X2 channel in this study because: (a) it desensitizes relatively slowly, thereby facilitating electrophysiological accessibility studies; (b) ion accessibility of the pore has been well characterized (Li et al., 2008, 2010; Kracun et al., 2010); and (c) it has high sequence identity to zfP2X4 in the transmembrane and extracellular regions (~50% identity). To facilitate subsequent computational analysis and experiments, we also created an rP2X2 homology model based on the closed-state zfP2X4 structure.

Electrostatic free energy of cations along the potential pathways in the closed state

To assess the energetics of ions along the two pathways, we calculated the electrostatic free energy of transferring Na^+ or Ca^{2+} from aqueous solution to the central pore of zfP2X4. The electrostatic free energy profile, shown in Fig. 2 A, includes both the static field arising from the protein charges, as well as the reaction field resulting from the different dielectric regions. In this closed-state

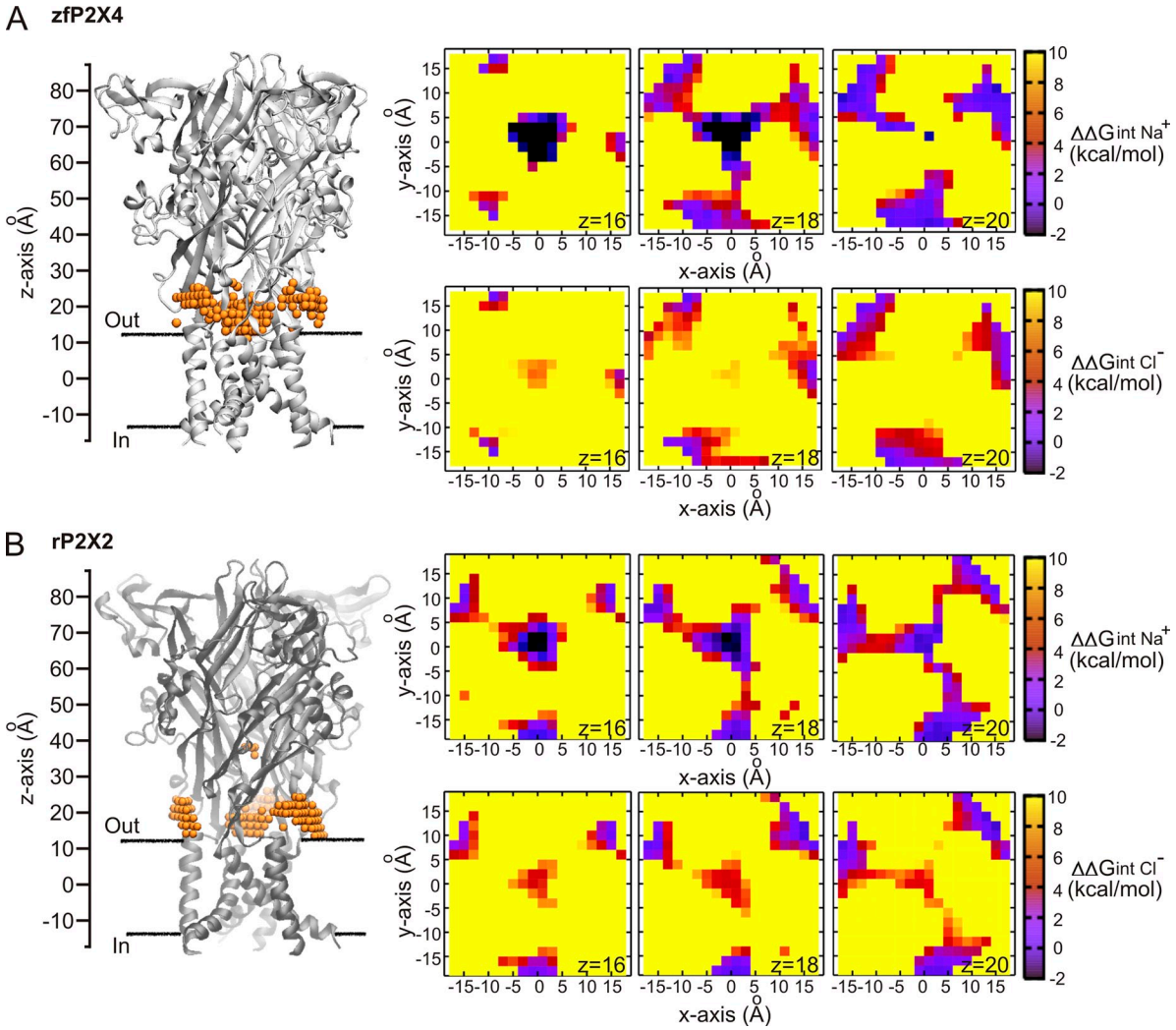

Figure 3. Electrostatic interaction free energy of ions along the lateral fenestrations in zfP2X4 and rP2X2. Results for zfP2X4 are shown in A, whereas those for rP2X2 are shown in B. The ion-accessible positions are shown as orange spheres near the extracellular membrane interface around Z = 15–25 Å (left). Free energy plots ($\Delta\Delta G_{int}$) for cross sections through the lateral fenestrations (Z = 16, 18, and 20 Å) are shown on the right for Na^+ (top) and Cl^- (bottom). Black squares indicate $\Delta\Delta G_{int} < -2$ Kcal mol^{-}.

Downloaded from http://rupress.org/jgp/article-pdf/137/6/579/1914952/jgp_201010593.pdf by guest on 10 February 2026

structure, the interaction energy of cations is prohibitive near the extracellular entrance of the central pathway (55 Å < Z < 85 Å). In contrast, the center of the extracellular domain (30 Å < Z < 55 Å) is extremely favorable for both Na^+ and Ca^{2+}, whereas the energy of Cl^- is repulsive at each point along the central axis. Both of these observations result from a strongly electronegative vestibule, lined by six negative residues (E98 and D99), which corresponds to the Gd^{3+}-binding site in the zfP2X4 structure. A simple expanded pore model was created to probe the degree of widening needed to reduce the electrostatic reaction field barrier and assess the static charge contribution to ion-interaction energies at the central axis. This was done by imposing a repulsive cylindrical potential restraint at the center of the pore and carrying out energy minimizations of the structure while successively increasing the cylinder radius. The resultant model has a pore that is 10 Å in diameter and maintains the overall distribution of residues lining the pore in the closed structure. In this model, the electrostatic free energy for Na^+ is favorable along most of the central pathway (Fig. 2 B), making it a possible pathway for cation permeation in zfP2X4. However, when we performed the same calculations for the rP2X2 homology model, there were still significant electrostatic barriers along the pore that occur because of the lack of acidic residues in the sequence of this homologue (Fig. 2, C and D). This suggests that although the central pathway is a favorable option in zfP2X4, the sequence variation in rP2X2 creates an unfavorable electrostatic environment that is unlikely to support cations along the central axis.

The electrostatic accessibility of the lateral fenestrations was also examined in the zfP2X4 structure and rP2X2 model (Fig. 3, A and B). We found that for both of these closed structures, there was a clear pathway connecting the outside solution to the central pore that

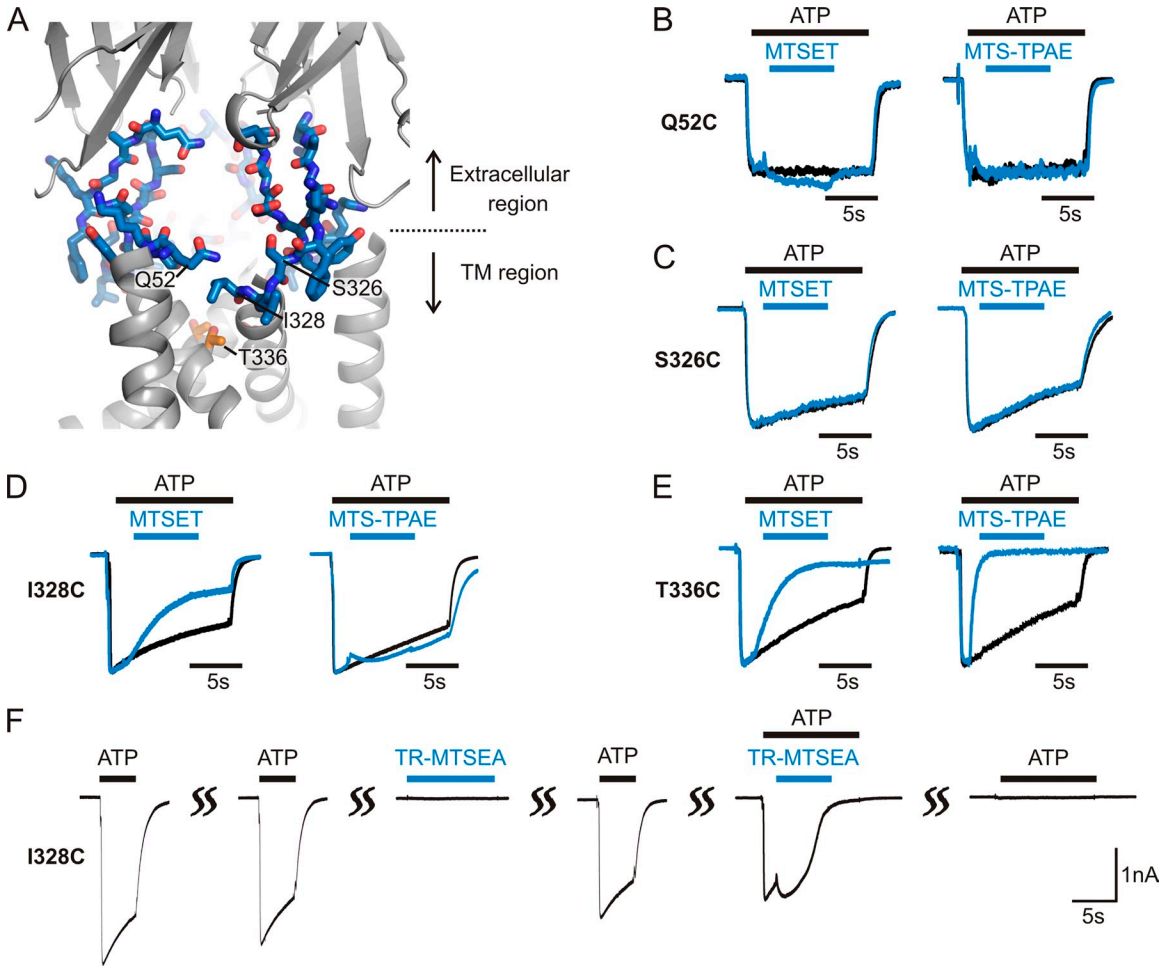

Figure 4. Accessibility of MTS reagents along the lateral fenestration. (A) The mutated residues are shown in stick representation (blue, carbon atoms; red, oxygen; dark blue, nitrogen), and the remaining region is shown in cartoon representations (gray). A transmembrane pore-lining residue, T336, is shown in orange. Representative residues are labeled. (B–E) Accessibility of two different-size MTS reagents in the presence of ATP. Superimposed scaled current traces recorded in response to ATP without (black) and with (blue) MTSET or MTS-TPAE applications (blue bars) show no modification for Q52C (B) and S326C (C), and modification for I328C (D) and T336C (E). (F) TR-MTSEA is accessible to I328C in the open state but not in the closed state. Exposing the channels to TR-MTSEA for 10 s in the closed state did not modify the ATP-induced current, whereas a 6-s exposure in the presence of ATP modified the current.

Downloaded from http://rupress.org/jgp/article-pdf/137/6/579/1914952/jgp_201010593.pdf by guest on 10 February 2026

was electrostatically accessible by Na^+ (<1 kcal mol^{-1}). Notably, Cl^- was not energetically stable along these pathways. Small openings of the windows would be sufficient to remove any small electrostatic barriers created by the protein reaction field and provide an energetically favorable pathway for cations. These calculations suggest that it is electrostatically possible for cations to move via the lateral fenestrations, even in the closed-state structure of both zfP2X4 and rP2X2.

Accessibility and structural changes around the lateral fenestrations

The lateral fenestrations consist of two strands connecting the two membrane-spanning α helices within each subunit to the large extracellular ligand-binding region. In contrast to the long and narrow central pathway, these lateral fenestrations are relatively wide and shallow in the closed-state structure (Fig. 1 B). We set out to explore whether these lateral fenestrations serve as ion permeation pathways by substituting Cys residues at each of the 17 residues that make up the walls of the fenestrations (Fig. 4 A), and tested whether their reaction with MTS reagents has detectable effects on ATP-activated currents. In the closed-state structure, these residues exhibit extensive solvent exposure and therefore should react with MTS reagents. However, if the wide and shallow features of the lateral fenestrations are maintained in the open state, one might imagine that MTS reagents would not have a dramatic effect on ion conduction, but might alter gating of the channel because these strands connect the ligand-binding region to the pore of the channel. For these experiments, we externally applied 2-(trimethylammonium)ethyl MTS (MTSET; mol wt: 278 D) and 2-(tripentylammonium)ethyl MTS (MTS-TPAE; mol wt: 447 D), two different-size reagents that are water soluble, membrane impermeable, and positively charged. Because both reagents react relatively rapidly with T336C within the gate region of rP2X2 in the presence of ATP ($\sim 10^4$ $M^{-1}s^{-}$), and cause reductions of ATP-induced currents (Fig. 4 E) (Li et al., 2008, 2010), the extracellular pathway to the pore must be wide enough for these MTS reagents to access the ion permeation pathway.

We examined the effects of these two MTS reagents on ATP-activated currents for each of the 15 Cys mutants that retained functional activity when expressed in HEK cells. Y55C and Q56C failed to form functional channels and were not studied further. Whole cell patch clamp recordings from these mutants revealed that the application of either MTSET or MTS-TPAE has negligible effects for most Cys mutants (Figs. 4, B and C, and 5 B). Modest current reduction was observed with MTSET for the I328C mutant (Fig. 4 D, left traces), whereas small current potentiation was recorded with MTS-TPAE (Fig. 4 D, right traces), suggesting that I328 in the lateral fenestration is accessible to both MTS reagents. The rate of MTSET modification at I328C was $\sim 5 \times 10^2$ $M^{-1}s^{-1}$ (n = 8), slower than the rates observed for MTSET modification of most pore-lining residues within TM2. Consistent with our expectations from the zfP2X4 structure, these results demonstrate that only one residue forming the lateral fenestrations exhibits detectable reaction with MTS reagents.

Although the zfP2X4 structure shows that the residues we tested in the lateral fenestrations are solvent exposed, and therefore should react with MTS reagents, an alternate possibility is that these lateral fenestrations collapse when the channel opens and their solvent accessibility decreases. To test this possibility, we examined whether the larger mushroom-shaped Texas red-2-sulfonamidoethyl MTS (TR-MTSEA; mol wt: 744 D) can react with I328C in either the absence or presence of ATP. Although TR-MTSEA does not react with I328C in the absence

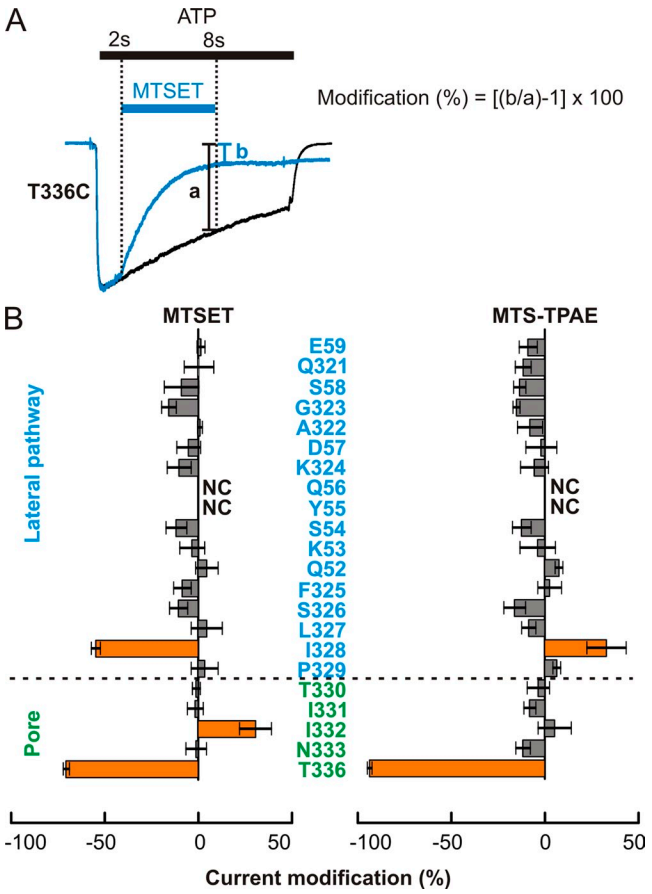

Figure 5. Quantitative comparisons of current modifications by MTS reagents along the lateral window. (A) Superimposed current traces of T336C recorded in response to ATP without (black) and with (blue) MTSET application (blue bar) using a 2-min interval between traces to illustrate how modification is quantified. Traces were scaled using the current amplitude 1.5 s after ATP application. Percent modification was calculated according to: modification (%) = [(b/a)−1] × 100, where b is the normalized current after a 6-s MTSET application, and a is the current at the corresponding time in the control trace. (B) Averaged current modifications by MTSET (left) or MTS-TPAE (right) at each Cys mutant (n = 3–9). Error bars are SEM. Orange bars indicate positions where current reduction or potentiation was observed.

Downloaded from http://rupress.org/jgp/article-pdf/137/6/579/1914952/jgp_201010593.pdf by guest on 10 February 2026

of ATP, consistent with its large size (~6 × 13 × 16 Å) and the dimensions of the lateral fenestrations in the closed-state zfP2X4 structure, it reacts rapidly in the presence of ATP (Fig. 4 F). Interestingly, the reagent initially potentiates ATP-activated current, similar to MTS-TPAE, but then causes complete inhibition of ATP-activated currents. One possible explanation is that the reaction with each subunit stabilizes the open state of the pore while occluding a lateral fenestration, and that complete inhibition is not detected until all three fenestrations are blocked. Regardless of the precise mechanisms, these results suggest that the lateral fenestrations become larger upon ATP binding; therefore, it is a likely pathway for ions to enter and exit the pore.

Accessibility and structural changes in the central pathway

To explore whether the central pathway might serve as a permeation pathway, we introduced Cys residues at 26 positions (Fig. 6 A) corresponding to residues at the central threefold axis in the zfP2X4 structure and tested for modification by MTS reagents. For 24 of these positions, both MTSET and MTS-TPAE had no effect on ATP-activated currents (Figs. 6, B–E, and 7 C). In the acidic central vestibule along the central pathway, two mutants (I317C and H319C) were modified by MTSET, but not by the larger MTS-TPAE. For I317C, MTSET increased the rate of deactivation (Fig. 7 A, middle traces), whereas for H319C, MTSET potentiated the ATP-induced current by ~40% and slowed the rate of current deactivation (Fig. 7 B, middle traces). In the case of I317C, subsequent application of ATP 3 min after the removal of MTSET resulted in ATP-activated currents that retained rapid deactivation, suggesting that the initial effects of MTSET are the result of covalent modification of I317C (Fig. 7 A, right traces). In the case of H319C, the potentiation of ATP-activated currents by MTSET did not recover after the removal of the MTS reagent, and a subsequent application of MTSET in the presence of ATP was without effect (Fig. 7 B, right traces), indicating covalent modification of H319C by MTSET. The rate of MTSET modification at H319C was $\sim 3.5 \times 10^3\ M^{-1}s^{-1}$ ($n = 5$), consistent with this residue being solvent exposed in the presence of ATP. In both cases, preapplication of MTS-TPAE did not affect the MTSET-dependent current modification (Fig. 7, A and B, left and middle traces), suggesting that the larger MTS-TPAE cannot access these residues.

To explore whether the central pathway undergoes a large conformational change upon ATP binding to create a wide route for extracellular ions to permeate, we engineered five pairs of double Cys mutants along the central pathway (Fig. 8 A), which based on the closed-state zfP2X4 structure would be predicted to form intersubunit disulfide bonds. Because P2X receptors are trimers, each Cys pair could give rise to a total of three disulfides. Such bridges should prevent a large motion because of conformational restraints caused by introducing intersubunit disulfide bridges. These double Cys mutants were expressed in HEK cells, and their ability to form disulfide bridges was assessed by SDS-PAGE in the absence of a reducing agent, followed by Western blotting.

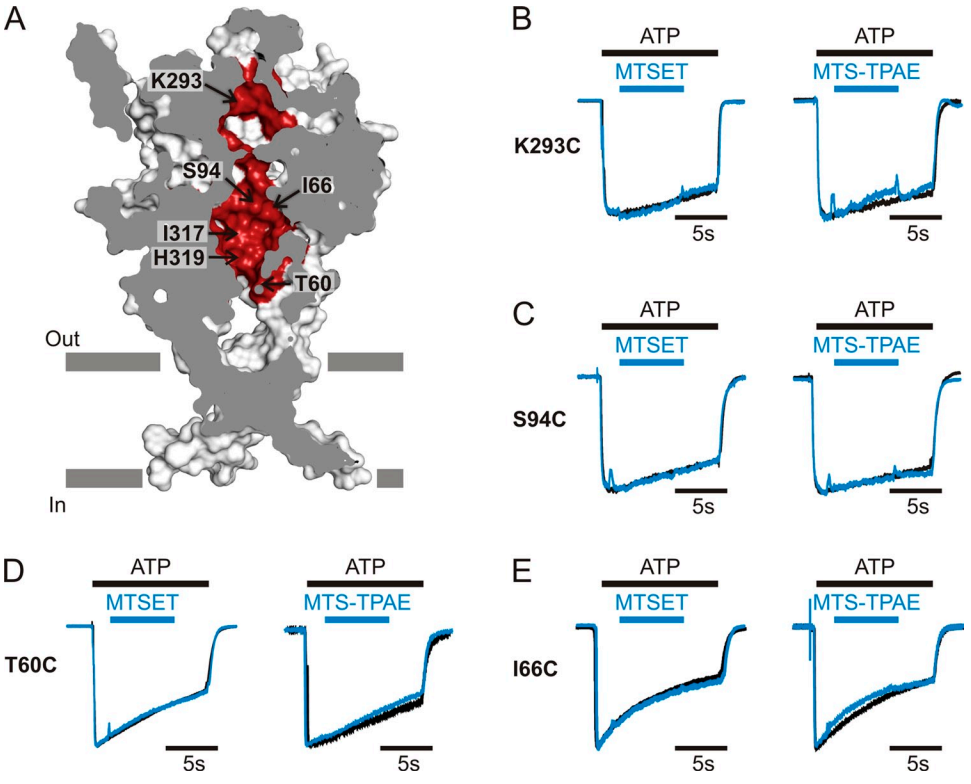

Figure 6. Accessibility of MTS reagents along the central pathway. (A) A sagittal section of a surface representation showing the mutated residues along the central pathway colored in red. Gray bars are predicted membrane leaflet. Representative residues are labeled. (B–E) Accessibility of two different-size MTS reagents in the open state. Superimposed scaled currents induced by ATP without (black) and with (blue) MTSET or MTS-TPAE applications (blue bars) show no modification for K293C (B), S94C (C), T60C (D), or I66C (E).

Downloaded from http://rupress.org/jgp/article-pdf/137/6/579/1914952/jgp_201010593.pdf by guest on 10 February 2026

Under mild air-oxidizing conditions, the band for the wild-type rP2X2 migrated at the appropriate molecular weight for the monomeric species (~53 kD), indicating that there is no intersubunit disulfide bridge formation in the parent construct (Fig. 8 B, lane WT). On the other hand, all double Cys mutants formed SDS-resistant trimers (~150 kD) or dimers (~100 kD), suggesting that intersubunit disulfides are formed, at least to some extent, in all the mutants (Fig. 8 B, lanes I–V).

Under identical air-oxidizing conditions, we performed whole cell patch clamp recordings from HEK cells expressing each pair of double Cys mutants. We chose to apply ATP (10 μM for the pairs I and III–V, and 30 μM for the pair II) for relatively short durations (1 s) at 2-min intervals because under these conditions, we observed relatively little rundown upon repeated applications of ATP (Fig. 9, left and middle traces). Notably, when cells were perfused with 10 mM DTT for 5 min to reduce disulfides, the top pair along the central pathway (Fig. 9, I) showed substantial current inhibition (~70%), whereas currents in three other pairs (II–IV) were unchanged. The data for bridge I indicate that the channel activity detected for the outer pair of Cys mutants under oxidizing conditions must be mediated, at least in part, by the Cys mutants whose subunits were covalently cross-linked by intersubunit disulfides. Thus, we conclude that restricting the subunit–subunit movements at the top of the central pathway is compatible with ion permeation through the rP2X2 channel, supporting the idea that a large opening of the central pathway is unlikely. The interpretation of the three bridges where DTT has no effect (Fig. 9, II–IV) is ambiguous because, as pointed out in the previous studies on K^+ channels (Kobertz et al., 2000), it is unclear whether the currents we observed are mediated by the population of disulfide cross-linked channels. We tried to drive disulfide bridge formation to completion by treating HEK cells with 0.3% H_2O_2 for 10 min, but no significant increase in disulfide formation was obtained (not depicted). In the case of the bottom pair (V), we observed large current potentiation when the cell was exposed to DTT, implying that the disulfide bond impairs a conformational change involved in channel opening. This bridge is actually positioned at the top of the lateral fenestration, and these results are therefore consistent with experiments with TR-MTSEA, which suggest that the lateral fenestrations become larger when the channel opens.

DISCUSSION

In this study, we explored the pathway for ions to permeate through the extracellular region of P2X receptor channels. The zfP2X4 crystal structure in the closed state reveals the presence of two potential pathways. Our Poisson-Boltzmann calculations suggest that substantial structural changes (>5 Å from the central axis) would be required for ions to permeate through the central

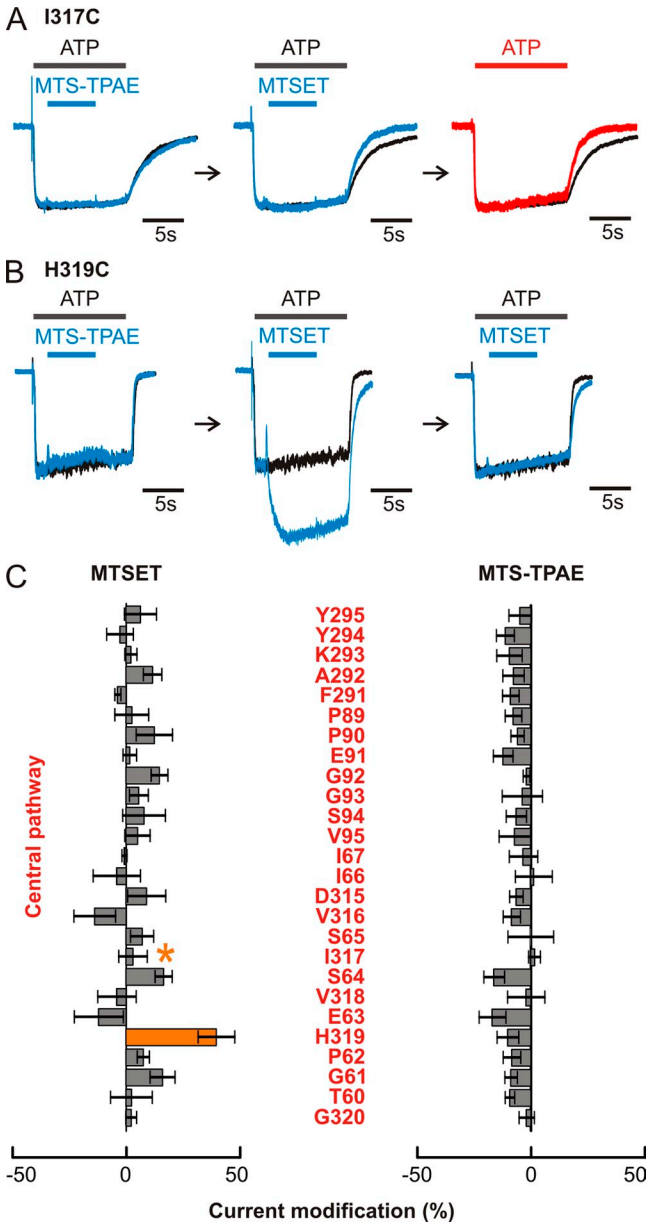

Figure 7. I317C and H319C in the central vestibule are accessible to MTSET but not to MTS-TPAE. Superimposed scaled current traces on the left show that extracellular application of MTS-TPAE (blue bar) has little effect on currents evoked by ATP (black bar). Extracellular application of MTSET, even after the application of MTS-TPAE, irreversibly modified currents evoked by ATP (right traces). (A) Deactivation of I317C mutant became faster after MTSET application. (B) ATP-induced current of H319C was potentiated by MTSET application. ATP was applied every 3 min. The control traces (black traces) in A and B are the same in each of the three panels. (C) Quantitative comparisons of current modifications by MTS reagents. Averaged current modifications by MTSET (left) or MTS-TPAE (right) at each Cys mutant (n = 3–9). Error bars are SEM. Orange bar highlights H319C, a position where MTSET causes pronounced current potentiation. Although I317C showed little change in current amplitude after MTSET application, the MTS reagent accelerated current deactivation after ATP removal; therefore, the residue is highlighted with an asterisk to indicate MTS reactivity.

Downloaded from http://rupress.org/jgp/article-pdf/137/6/579/1914952/jgp_201010593.pdf by guest on 10 February 2026

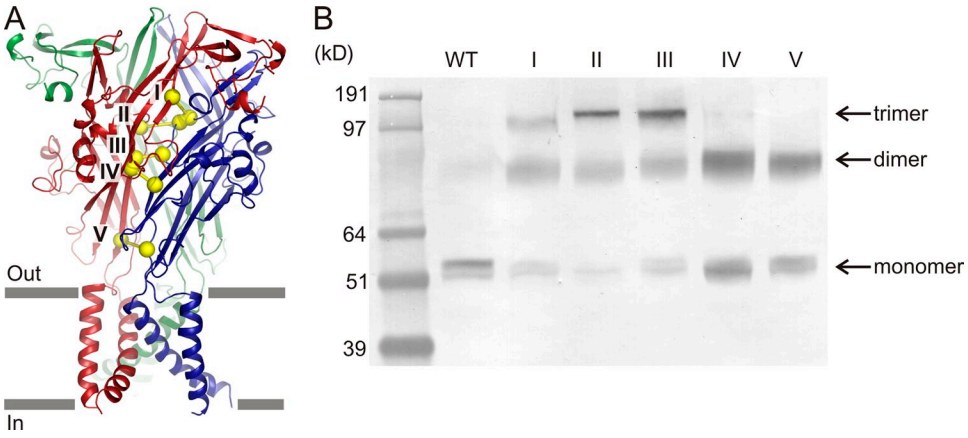

Figure 8. Restricting motion by introducing double Cys mutants that form intersubunit disulfide bridges. (A) Locations of the five double Cys mutants created in this study: I, P89C/F291C; II, G93C/V95C; III, P90C/E91C; IV, S65C/D315C; V, E59C/Q321C. For clarity, bridges are only shown for one of the three subunit interfaces. (B) Western blot in the absence of reducing agent indicates that all five mutants form either trimers or dimers.

pathway (Fig. 2). Although our accessibility experiments show that ions up to the size of MTSET can reach the central vestibule (Fig. 7), we failed to observe any modification of residues in the rest of the central pathway (Fig. 6). In addition, large MTS reagents like MTS-TPAE can readily access the transmembrane pore but cannot access either the central or upper vestibules (Figs. 6 and 7), suggesting that the central pathway is unlikely to be an ion permeation pathway. Importantly, engineered disulfide bridges that should constrain movement at the upper end of the central pathway do not significantly perturb channel function (Figs. 8 and 9), excluding the possibility that the central pathway undergoes a large dilation upon activation. In contrast, our computational analysis shows no significant electrostatic barriers for cations to enter from the lateral fenestrations (Fig. 3), and our accessibility results identify one position where both MTSET and MTS-TPAE can access an introduced Cys in the presence of ATP (Fig. 4).

Enlargement of the lateral fenestrations in the open state

One expectation of accessibility studies with ion channels is that the introduction of a positive charge with an MTS reagent should reduce macroscopic current if the Cys is positioned along a relatively narrow permeation pathway. These expectations were met in previous studies identifying pore-lining residues and the gate within TM2 of the rP2X2 receptor channel (Li et al., 2008, 2010). The relative scarcity of reactive positions within the central pathway in the present study is not surprising if it does not contribute to the ion permeation pathway. The central pathway is ~70-Å long and includes extended regions where packing within the protein minimizes its diameter, and at least at its outer end does not undergo a substantial structural change during gating, as inferred from the engineered disulfide that retains activity. However, after screening 15 Cys mutants within the lateral fenestrations with two different-size MTS reagents, we found only one mutant (I328C) that decreased ATP-induced current upon MTSET application (Fig. 4), and in this instance, the rate of modification was relatively

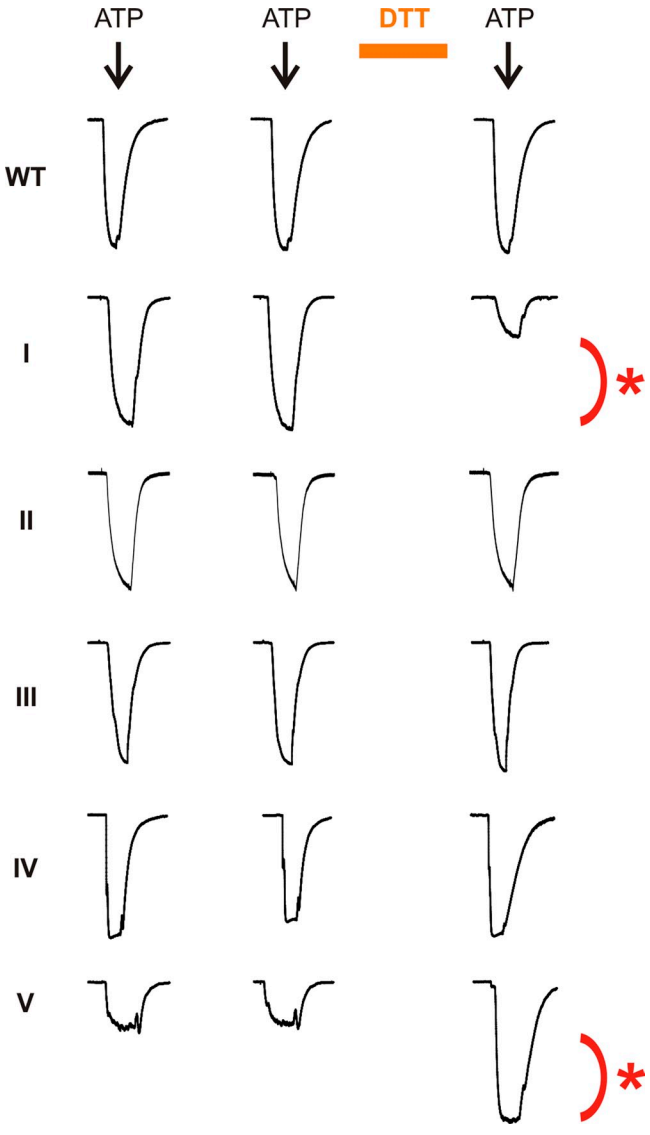

Figure 9. Disulfide bridge formation in the central pathway preserves channel activity. Two short pulses of ATP applications (1 s; black arrows) with 2-min intervals showed inward currents without significant rundown. External DTT application (5-min duration) reduced the current amplitude of the mutant pair I and potentiated mutant pair V (red asterisks).

Downloaded from http://rupress.org/jgp/article-pdf/137/6/579/1914952/jgp_201010593.pdf by guest on 10 February 2026

moderate ($\sim 5 \times 10^2$ $M^{-1}s^{-1}$). Although the modest modification rate could be the consequence of various local factors (e.g., dynamical, structural, or energetic) suppressing the reactive thiolate ion in this region, the lack of effect at the other 14 positions within the lateral fenestration suggests that the diameter of the opening is actually quite large in the open state. In this case, many of the functionally silent positions may have reacted with MTS reagents, but the size of the opening prevents the positive charge from attenuating ion throughput. This interpretation would be consistent with a recent MTS accessibility study on pannexin hemichannels (Wang and Dahl, 2010), which failed to identify any reactive positions within the four TM helices, even though the recent crystal structure of a potential structural analogue, the gap junction channel (Maeda et al., 2009), would predict many to be highly solvent exposed. Enlargement of the lateral fenestrations when P2X receptor channels open is strongly suggested by accessibility experiments with large MTS reagents like MTS-TPAE ($\sim 6 \times 12 \times 13$ Å) and Texas red ($\sim 6 \times 13 \times 16$ Å), which can rapidly enter the pore and react with pore-lining residues (Fig. 4) (Li et al., 2010), requiring that the fenestrations be significantly larger than these reagents. Indeed, our present experiment with TR-MTSEA and position I328C within the lateral fenestration suggests that it becomes larger as the channel opens. The breathing of the lateral fenestrations with opening would also be consistent with the effects of the intersubunit disulfide bridge in this region (V). Reduction of this bridge with DTT enhances macroscopic current (Figs. 8 and 9), suggesting that constraining motions of the lateral fenestration prevents the opening of the channel.

Ion selection in the lateral fenestrations

In identifying the lateral fenestration as the permeation pathway for ions to enter or exit the pore, it becomes interesting to consider whether this pathway may contribute to the ion selectivity of P2X receptor channels. Our Poisson-Boltzmann calculations reveal that the electrostatic interaction energy along this short (~15-Å) pathway is relatively favorable for Na^+ permeation ($\Delta\Delta G_{int}$ = −1 to +1 kcal mol^{-1}), but not for Cl^- ($\Delta\Delta G_{int}$ > +10 kcal mol^{-1}) (Fig. 3), suggesting that the overall negative potential in this area may contribute to selecting cations over anions. Interestingly, the P2X5 receptor has been reported to also be permeable to anions (pCl^-/pNa^+ = ~0.5; Ruppelt et al., 2001; Bo et al., 2003), and the electrostatic potential in a hP2X5 receptor homology model is significantly positive around the lateral fenestration (~+10 kcal mol^{-1}; Fig. 10), supporting the hypothesis that the electrostatics along the lateral fenestration plays a role in ion selection.

Role of the acidic central vestibule

Why do P2X receptors contain a large acidic vestibule in the middle of the central pathway? In our MTS accessibility studies, we found that the smaller MTSET ($\sim 6 \times 6 \times 10$ Å) can access the acidic central vestibule through the lateral fenestrations and potentiates currents (H319C) or accelerates the rate of deactivation (I317C) (Fig. 7, A and B). These data suggest that extracellular ions can reach the central vestibule and allosterically modulate conformational changes in the extracellular domain involved in opening the pore. Supporting this, a trivalent cation (Gd^{3+}) has been shown to bind in the central vestibule of zfP2X4 and inhibit ATP-induced

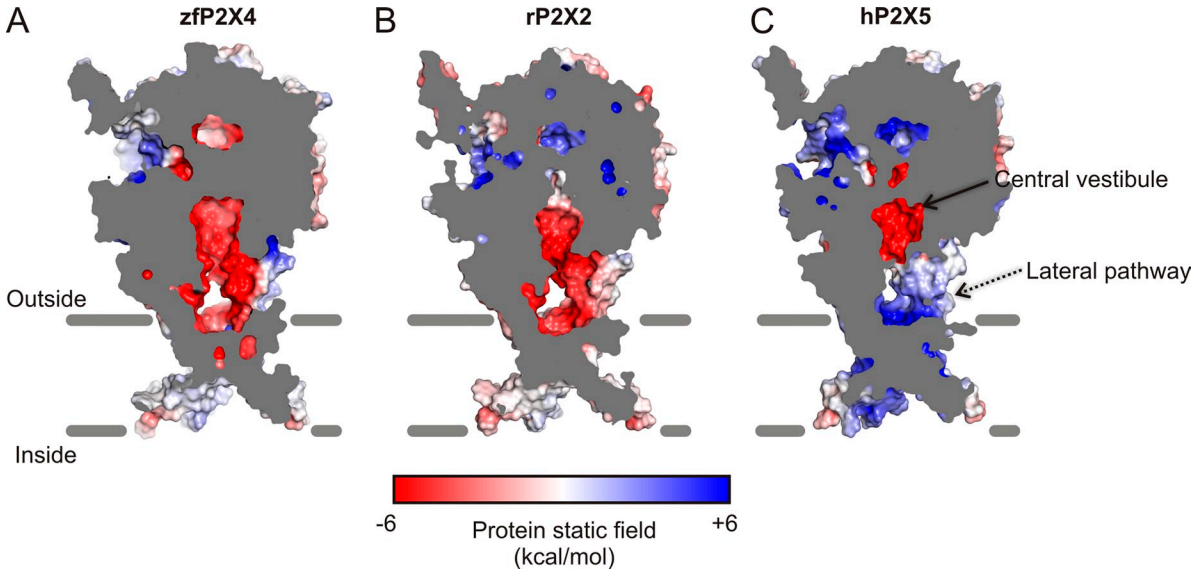

Figure 10. Electrostatic potential in the lateral fenestrations may contribute to selecting cations over anions. Sagittal sections of the electrostatic potential surface calculated using the APBS tools (Baker et al., 2001). (A) zfP2X4 with supplemented side chains. Homology models of rP2X2 (B) and hP2X5 (C). Surface is colored based on the potential, contoured from −6 kcal mol^{-1} (red) to +6 kcal mol^{-1} (blue). White denotes 0 kcal mol^{-1}.

Downloaded from http://rupress.org/jgp/article-pdf/137/6/579/1914952/jgp_201010593.pdf by guest on 10 February 2026

currents (Kawate et al., 2009). It is also tempting to speculate that the acidic surface may serve a role in concentrating cations, facilitating their influx to the transmembrane pore. Interestingly, previous studies have shown that in large-conductance Ca^{2+}-activated K^+ (BK) and KcsA K^+ channels, intracellular K^+ is locally concentrated by a ring of negatively charged glutamate residues at the entrance of the intracellular vestibule (Brelidze et al., 2003; Nimigean et al., 2003). In the study on BK channels, the local concentration of K^+ at the internal mouth of the pore is estimated (based on the reversal potentials) to increase from 150 to 500 mM as a result of the negative charges. If the central vestibule in the extracellular region of a P2X receptor increases the local concentration of Na^+ in a similar manner to BK channels, this acidic central vestibule should have a profound effect on cation/anion selectivity.

We thank Charu Chaudhry, Joe Mindell, Mark Mayer, Justin Taraska, and members of the Swartz laboratory for helpful discussions, and Chris Miller for generosity with computational resources.

This work was supported by the Intramural Research Program of the National Institute of Neurological Disorders and Stroke, National Institutes of Health (NIH; to K.J. Swartz), and NIH Pathway to Independence awards to T. Kawate (NS 072869) and M. Li (NS 070954). J.L. Robertson was supported by funding from the Howard Hughes Medical Institute.

Richard W. Aldrich served as editor.

Submitted: 29 December 2010
Accepted: 10 May 2011

REFERENCES

Baker, N.A., D. Sept, S. Joseph, M.J. Holst, and J.A. McCammon. 2001. Electrostatics of nanosystems: application to microtubules and the ribosome. *Proc. Natl. Acad. Sci. USA.* 98:10037–10041. doi:10.1073/pnas.181342398

Bo, X., L.H. Jiang, H.L. Wilson, M. Kim, G. Burnstock, A. Surprenant, and R.A. North. 2003. Pharmacological and biophysical properties of the human P2X5 receptor. *Mol. Pharmacol.* 63:1407–1416. doi:10.1124/mol.63.6.1407

Brelidze, T.I., X. Niu, and K.L. Magleby. 2003. A ring of eight conserved negatively charged amino acids doubles the conductance of BK channels and prevents inward rectification. *Proc. Natl. Acad. Sci. USA.* 100:9017–9022. doi:10.1073/pnas.1532257100

Brooks, B.R., C.L. Brooks III, A.D. Mackerell Jr., L. Nilsson, R.J. Petrella, B. Roux, Y. Won, G. Archontis, C. Bartels, S. Boresch, et al. 2009. CHARMM: the biomolecular simulation program. *J. Comput. Chem.* 30:1545–1614. doi:10.1002/jcc.21287

Burnstock, G. 2006. Historical review: ATP as a neurotransmitter. *Trends Pharmacol. Sci.* 27:166–176. doi:10.1016/j.tips.2006.01.005

Chessell, I.P., J.P. Hatcher, C. Bountra, A.D. Michel, J.P. Hughes, P. Green, J. Egerton, M. Murfin, J. Richardson, W.L. Peck, et al. 2005. Disruption of the P2X7 purinoceptor gene abolishes chronic inflammatory and neuropathic pain. *Pain.* 114:386–396. doi:10.1016/j.pain.2005.01.002

Cook, S.P., L. Vulchanova, K.M. Hargreaves, R. Elde, and E.W. McCleskey. 1997. Distinct ATP receptors on pain-sensing and stretch-sensing neurons. *Nature.* 387:505–508. doi:10.1038/387505a0

Dell'Antonio, G., A. Quattrini, E. Dal Cin, A. Fulgenzi, and M.E. Ferrero. 2002. Antinociceptive effect of a new P(2Z)/P2X7 antagonist, oxidized ATP, in arthritic rats. *Neurosci. Lett.* 327:87–90. doi:10.1016/S0304-3940(02)00385-3

Dowd, E., D.S. McQueen, I.P. Chessell, and P.P. Humphrey. 1998. P2X receptor-mediated excitation of nociceptive afferents in the normal and arthritic rat knee joint. *Br. J. Pharmacol.* 125:341–346. doi:10.1038/sj.bjp.0702080

Eswar, N., B. Webb, M.A. Marti-Renom, M.S. Madhusudhan, D. Eramian, M.Y. Shen, U. Pieper, and A. Sali. 2006. Comparative protein structure modeling using Modeller. *Curr. Protoc. Bioinformatics.* 15: 5.6.1–5.6.30.

Finger, T.E., V. Danilova, J. Barrows, D.L. Bartel, A.J. Vigers, L. Stone, G. Hellekant, and S.C. Kinnamon. 2005. ATP signaling is crucial for communication from taste buds to gustatory nerves. *Science.* 310:1495–1499. doi:10.1126/science.1118435

Idzko, M., H. Hammad, M. van Nimwegen, M. Kool, M.A. Willart, F. Muskens, H.C. Hoogsteden, W. Luttmann, D. Ferrari, F. Di Virgilio, et al. 2007. Extracellular ATP triggers and maintains asthmatic airway inflammation by activating dendritic cells. *Nat. Med.* 13:913–919. doi:10.1038/nm1617

Im, W., D. Beglov, and B. Roux. 1998. Continuum solvation model: computation of electrostatic forces from numerical solutions to the Poisson-Boltzmann equation. *Comput. Phys. Commun.* 111:59–75. doi:10.1016/S0010-4655(98)00016-2

Johnson, J.P. Jr., and W.N. Zagotta. 2005. The carboxyl-terminal region of cyclic nucleotide-modulated channels is a gating ring, not a permeation path. *Proc. Natl. Acad. Sci. USA.* 102:2742–2747. doi:10.1073/pnas.0408323102

Kawate, T., J.C. Michel, W.T. Birdsong, and E. Gouaux. 2009. Crystal structure of the ATP-gated P2X(4) ion channel in the closed state. *Nature.* 460:592–598. doi:10.1038/nature08198

Kobertz, W.R., and C. Miller. 1999. K+ channels lacking the 'tetramerization' domain: implications for pore structure. *Nat. Struct. Biol.* 6:1122–1125. doi:10.1038/70061

Kobertz, W.R., C. Williams, and C. Miller. 2000. Hanging gondola structure of the T1 domain in a voltage-gated K(+) channel. *Biochemistry.* 39:10347–10352. doi:10.1021/bi001292j

Kracun, S., V. Chaptal, J. Abramson, and B.S. Khakh. 2010. Gated access to the pore of a P2X receptor: structural implications for closed-open transitions. *J. Biol. Chem.* 285:10110–10121. doi:10.1074/jbc.M109.089185

Li, M., T.H. Chang, S.D. Silberberg, and K.J. Swartz. 2008. Gating the pore of P2X receptor channels. *Nat. Neurosci.* 11:883–887. doi:10.1038/nn.2151

Li, M., T. Kawate, S.D. Silberberg, and K.J. Swartz. 2010. Pore-opening mechanism in trimeric P2X receptor channels. *Nat Commun.* 1:44.

Long, S.B., X. Tao, E.B. Campbell, and R. MacKinnon. 2007. Atomic structure of a voltage-dependent K+ channel in a lipid membrane-like environment. *Nature.* 450:376–382. doi:10.1038/nature06265

Maeda, S., S. Nakagawa, M. Suga, E. Yamashita, A. Oshima, Y. Fujiyoshi, and T. Tsukihara. 2009. Structure of the connexin 26 gap junction channel at 3.5 A resolution. *Nature.* 458:597–602. doi:10.1038/nature07869

Nicke, A., H.G. Bäumert, J. Rettinger, A. Eichele, G. Lambrecht, E. Mutschler, and G. Schmalzing. 1998. P2X1 and P2X3 receptors form stable trimers: a novel structural motif of ligand-gated ion channels. *EMBO J.* 17:3016–3028. doi:10.1093/emboj/17.11.3016

Nimigean, C.M., J.S. Chappie, and C. Miller. 2003. Electrostatic tuning of ion conductance in potassium channels. *Biochemistry.* 42:9263–9268. doi:10.1021/bi0348720

Nina, M., D. Beglov, and B. Roux. 1997. Atomic radii for continuum electrostatics calculations based on molecular dynamics free energy simulations. *J. Phys. Chem. B.* 101:5239–5248. doi:10.1021/jp970736r

Downloaded from http://rupress.org/jgp/article-pdf/137/6/579/1914952/jgp_201010593.pdf by guest on 10 February 2026

Nishida, M., and R. MacKinnon. 2002. Structural basis of inward rectification: cytoplasmic pore of the G protein-gated inward rectifier GIRK1 at 1.8 A resolution. *Cell.* 111:957–965. doi:10.1016/S0092-8674(02)01227-8

Nishida, M., M. Cadene, B.T. Chait, and R. MacKinnon. 2007. Crystal structure of a Kir3.1-prokaryotic Kir channel chimera. *EMBO J.* 26:4005–4015. doi:10.1038/sj.emboj.7601828

North, R.A. 2002. Molecular physiology of P2X receptors. *Physiol. Rev.* 82:1013–1067.

Reynolds, J.A., and A. Karlin. 1978. Molecular weight in detergent solution of acetylcholine receptor from Torpedo californica. *Biochemistry.* 17:2035–2038. doi:10.1021/bi00604a001

Robertson, J.L., L.G. Palmer, and B. Roux. 2008. Long-pore electrostatics in inward-rectifier potassium channels. *J. Gen. Physiol.* 132:613–632. doi:10.1085/jgp.200810068

Rosenmund, C., Y. Stern-Bach, and C.F. Stevens. 1998. The tetrameric structure of a glutamate receptor channel. *Science.* 280:1596–1599. doi:10.1126/science.280.5369.1596

Ruppelt, A., W. Ma, K. Borchardt, S.D. Silberberg, and F. Soto. 2001. Genomic structure, developmental distribution and functional properties of the chicken P2X(5) receptor. *J. Neurochem.* 77:1256–1265. doi:10.1046/j.1471-4159.2001.00348.x

Sobolevsky, A.I., M.P. Rosconi, and E. Gouaux. 2009. X-ray structure, symmetry and mechanism of an AMPA-subtype glutamate receptor. *Nature.* 462:745–756. doi:10.1038/nature08624

Solle, M., J. Labasi, D.G. Perregaux, E. Stam, N. Petrushova, B.H. Koller, R.J. Griffiths, and C.A. Gabel. 2001. Altered cytokine production in mice lacking P2X(7) receptors. *J. Biol. Chem.* 276:125–132. doi:10.1074/jbc.M006781200

Souslova, V., P. Cesare, Y. Ding, A.N. Akopian, L. Stanfa, R. Suzuki, K. Carpenter, A. Dickenson, S. Boyce, R. Hill, et al. 2000. Warm-coding deficits and aberrant inflammatory pain in mice lacking P2X3 receptors. *Nature.* 407:1015–1017. doi:10.1038/35039526

Tao, X., J.L. Avalos, J. Chen, and R. MacKinnon. 2009. Crystal structure of the eukaryotic strong inward-rectifier K+ channel Kir2.2 at 3.1 A resolution. *Science.* 326:1668–1674. doi:10.1126/science.1180310

Tsuda, M., Y. Shigemoto-Mogami, S. Koizumi, A. Mizokoshi, S. Kohsaka, M.W. Salter, and K. Inoue. 2003. P2X4 receptors induced in spinal microglia gate tactile allodynia after nerve injury. *Nature.* 424:778–783. doi:10.1038/nature01786

Unwin, N. 2005. Refined structure of the nicotinic acetylcholine receptor at 4 A resolution. *J. Mol. Biol.* 346:967–989. doi:10.1016/j.jmb.2004.12.031

Vial, C., J.A. Roberts, and R.J. Evans. 2004. Molecular properties of ATP-gated P2X receptor ion channels. *Trends Pharmacol. Sci.* 25:487–493. doi:10.1016/j.tips.2004.07.008

Wang, J., and G. Dahl. 2010. SCAM analysis of Panx1 suggests a peculiar pore structure. *J. Gen. Physiol.* 136:515–527. doi:10.1085/jgp.201010440

Downloaded from http://rupress.org/jgp/article-pdf/137/6/579/1914952/jgp_201010593.pdf by guest on 10 February 2026